Single nucleon removal in relativistic nuclear collisions

C. J. Benesh, B. C. Cook, and J. P. Vary
Physics Department, Iowa State University, Ames, Iowa 50011
(Received 1 May 1989)

We implement a simple approach to the inclusive cross section for single nucleon removal by relativistic nucleons and nuclei. We first develop the projectile and target dependence of the mean number, $N(b)$, of nucleon-nucleon collisions as a function of impact parameter in the peripheral region. Using the Glauber approximation, we obtain a simple parametrization for a critical impact parameter b_c such that the reaction cross sections for both N-B and A-B collisions are well represented by πb_c^2. Further study of the b dependence of $N(b)$ around $b=b_c$ allows us to develop a parametrization of single nucleon abrasion cross sections. Next, we employ the Weizsacker-Williams approximation with b_c as the cutoff impact parameter to calculate the Coulomb contribution to the single nucleon removal process. The results are compared with recent data which suggest that the Weizsacker-Williams approximation is inadequate for heavy projectiles. Using our estimates for the nuclear contribution, we find that the data yields good agreement with the Weizsacker-Williams results for virtually all projectile-target combinations. We therefore conclude that the measured deviations from the Weizsacker-Williams results do not represent new physics, but rather reflect uncertainties in the estimation of the nuclear contribution to the single nucleon removal process. As an elementary example of the possible new physics that may be observed in this process, we calculate the contributions from a coherent nuclear process and the possible interference effects. For heavy projectiles, we find that the interference effects are comparable to the present experimental uncertainties.

I. INTRODUCTION

Single nucleon removal by a high-energy particle has long been studied with radiochemical techniques, and the Coulomb dissociation cross section has been inferred.[1] Simple models[2] for these large cross sections have been developed in order that deviations from the model predictions may be isolated. Recently, deviations from model predictions have been reported for high-Z projectiles.[3] These measurements seem to indicate that the simple Weizsacker-Williams (WW) approximation used to calculate the Coulomb contribution to the cross section is inadequate for heavy projectiles. In this paper, we examine the sensitivity of these results to the model used to calculate the nuclear contribution to the cross section, and develop an approach capable of addressing coherent Coulomb-nuclear interference effects.

The plan of this paper is as follows. Section II reviews the Glauber approximation for the mean number of nucleon-nucleon collisions. A simple parametrization of the incoherent abrasion component of the single nucleon removal cross section emerges. In Sec. III, we describe the corrections to the Glauber treatment arising from final state interactions (FSI) and present comparisons with model results at 400 MeV and 2.1 GeV. Section IV consists of a presentation of the Weizsacker-Williams approximation, and a simple WW inspired model for calculating nuclear-Coulomb interference effects. In Sec. V, we compare model calculations with experimental data, and find that reasonable agreement is obtained. Finally, in Sec. VI, we discuss these results and present our conclusions.

II. SYSTEMATICS OF THE GLAUBER APPROXIMATION

A. Reaction cross sections

As a well-known approximation to nucleon-nucleus and nucleus-nucleus cross sections, the Glauber approach[4,5] obtains the reaction cross section σ_{AB}^R as an integral over impact parameters

$$\sigma_{AB}^R = 2\pi \int b\, db \{1-\exp[-4\,\mathrm{Im}\chi_{AB}(b)]\} , \tag{1}$$

where A and B represent the atomic number of the projectile and target, respectively, and

$$\chi_{AB}(b) = (i+\beta)\frac{\sigma}{4} T(b) \tag{2}$$

with

$$T(b) = \int dz \int d^3r' \rho_A(\mathbf{r}-\mathbf{r}')\rho_B(\mathbf{r}') . \tag{3}$$

In the above equation, σ represents the nucleon-nucleon cross section taken at the same incident laboratory energy per nucleon, β is the ratio of the real to imaginary forward nucleon-nucleon scattering amplitude, and ρ_A and ρ_B are the projectile and target mass densities normalized to A and B, respectively. Throughout our calculations, we will neglect the differences between neutron and proton density distributions.

A number of studies[6-12] have employed (1) to discuss the geometrical aspects of nucleon-nucleon collisions. In particular, it has been quite popular to compare the results of (1) with the classical geometric cross section

$$\sigma_{AB}^{\text{class}}=\pi(r_A+r_B)^2=\pi r_0^2(A^{1/3}+B^{1/3})^2 . \quad (4)$$

A fit to a variety of Glauber results at 2.1 GeV/nucleon gave $r_0=1.27$ fm.[10] It should be noted, however, that this parametrization is inadequate for cases involving lighter nuclei. In addition, it does not correspond to the $A\rightarrow 1$ limit, where cosmic ray results have been used to determine the parameters of the Bradt-Peters formula[13]

$$\sigma_{1B}^{R}=\pi r_0^2(1+B^{1/3}-c)^2 . \quad (5)$$

The corrections to (4) involve overlap considerations and have been discussed in some detail in Ref. 12. Here, we prefer to take a simple, physically intuitive approach to the geometrical parametrization of the results of (1). We will then employ these results with densities taken from electron scattering data to provide the actual parameters of the geometrical form.

To accomplish this, we first recall that nucleon-nucleus and nucleus-nucleus collisions have long been interpreted in optical model studies as highly absorptive interactions. That is, little transparency is evident. In the multipole scattering picture, we argue that there is a critical impact parameter b_c inside which nuclear reactions will occur with high probability. This is controlled by the mean number $N(b)$ of nucleon-nucleon collisions as a function of impact parameter

$$N(b)=\sigma T(b) . \quad (6)$$

The function $N(b)$ should rise very rapidly from $N(b)\ll 1$ for $b>b_c$ to a value $N(b)>1$ for $b<b_c$. Thus, we argue that $N(b_c)\approx 0.5$ indicates the vicinity of a critical impact parameter b_c inside of which nearly all collisions will be inelastic. The reaction cross section is then expected to be

$$\sigma_R^{AB}=\pi b_c^2 . \quad (7)$$

We now seek a functional form of b_c motivated by the geometrical form (3) that fits a wide variety of projectile target combinations. For two identical, constant density spheres, Eq. (3) yields, in the limit $A\gg 1$,

$$b_c=2r_0(A^{1/3}-\alpha A^{-1/5}) , \quad (8)$$

where $R=r_0A^{1/3}$ is the radius of each sphere and α is a numerical constant. This limit is realized very slowly, however, and a much better parametrization to the solutions of $N(b)=0.5$ for $A<200$ is given by

$$b_c=2r_0(A^{1/3}-\alpha' A^{-1/10}) . \quad (9)$$

For more realistic matter distributions, we expect b_c to have an expansion in integral powers of the projectile and target radii and to be symmetric under interchange of the two. Thus, we postulate that, for large A,

$$b_c\approx r_0[A^{1/3}+B^{1/3}-x(A^{-1/3}+B^{-1/3})] . \quad (10)$$

The parameters r_0 and x will be treated as adjustable and determined by fits of (10) to actual calculations performed with Eqs. (1)–(3). We note in passing that analogous arguments have been made to obtain the "proximity type" optical potential between two nuclei.[14]

To obtain the best-fit values of the parameters r_0 and x we utilize all the nucleon-nucleus cases at 1.5 GeV of Ref. 11 and added eight more nucleus-nucleus cases at intermediate to large values of $A^{1/3}+B^{1/3}$. The densities are taken from the tabulation of fits of electron scattering data in Ref. 15 with the exceptions as noted in Ref. 11. The best-fit values obtained were $r_0=1.34$ fm and $x=0.75$. The calculated results of Eqs. (1)–(3) are displayed as discrete values in Fig. 1 as a function of b_c/r_0. We also show a smooth curve resulting from the parametrization (10). Overall, a very satisfactory fit from the lowest cross section ($p+{}^3$He) through the largest (^{238}U+^{238}U) is obtained. In addition, we display three nucleus-nucleus experimental results at 2.1 GeV/nucleon since negligible changes in the calculated results occur with increasing energy.[17] This independence of σ_R^{AB} to changes in σ on the order of 25% and large changes in β has been discussed in Refs. 12 and 13. Thus, for our purposes we will consider σ_R^{AB} as energy independent.

Having achieved a simple parametrization for σ_R^{AB}, we have defined a scale on which to study the function $N(b)$ that enters the Glauber calculations. This function differs markedly for the $p+{}^4$He and ^{20}Ne+^{238}U cases shown in Fig. 2. In the region around b_c, however, they are strikingly similar, as illustrated in Fig. 3. What is

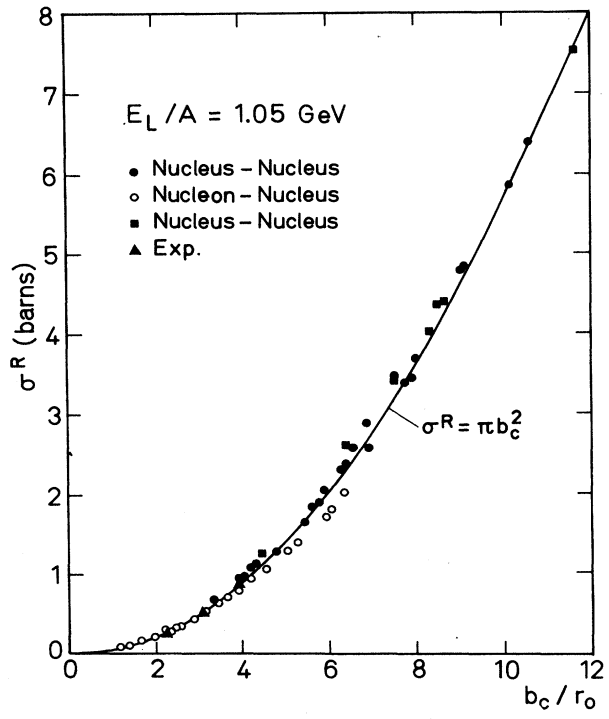

FIG. 1. Total reaction cross section for nucleon-nucleus and nucleus-nucleus interactions at 1.05 GeV/nucleon as a function of b_c/r_0. The parameters r_0 and x are determined by a least-squares fit to the cross section taken from Ref. 11. The solid squares represent new results obtained for this paper. The experimental results are from Ref. 16.

more impressive is that these two cases are *not* typical, and in fact represent the two cases chosen to be as different as possible. The absolute magnitude and slopes of $N(b)$ are nearly equal in both cases, and serve as indications of the typical behavior over a 1 fermi interval range around b_c. Our next task is to explore the possible universality of $N(b)$ and its first derivative around $b=b_c$. Physically, one might expect to find such universality as a consequence of the constancy of the central density and surface thickness for a wide range of nuclei. In Fig. 4, we have plotted the quantities $T(b_c)$ and $T'(b_c)\equiv\partial T/\partial b|_{b_c}$, with $b_c=(\sigma_R^{AB}/\pi)^{1/2}$, for all cases displayed in Fig. 1. Note the greatly expanded scale. Within 5%, these quantities are the same for all projectile-target combinations studied. [A slight decrease of $T'(b_c)$ is evident for $b_c\geq 8$ fm, but this effect is small.] The $p+{}^4$He and ^{20}Ne+^{238}U cases of Fig. 3 represents the two cases with the *largest slope difference* of all the cases studied. It is noteworthy that the average result for $T(b_c)$ corresponds to $N(b_c)=0.56$ for $\sigma=44$ mb, in rough agreement with the classical expectations described previously.

The conclusion we reach from these systematics is that the geometrical behavior of σ_R^{AB} can be used to determine a scale b_c useful for systematizing the results from peripheral collisions of a wide variety of projectile-target arrangements.

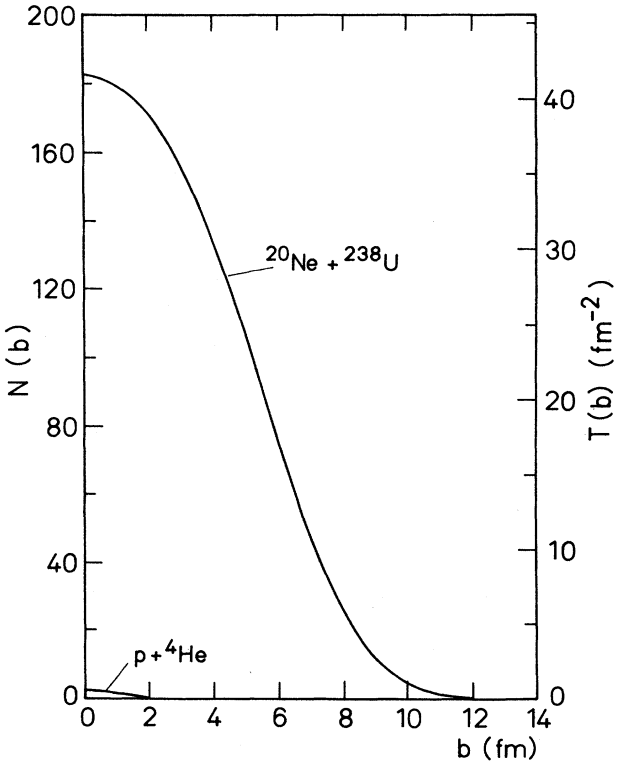

FIG. 2. Thickness functions $T(b)$ and average number of nucleon-nucleon collisions $N(b)$ as a function of impact parameter for two widely different projectile-target arrangements.

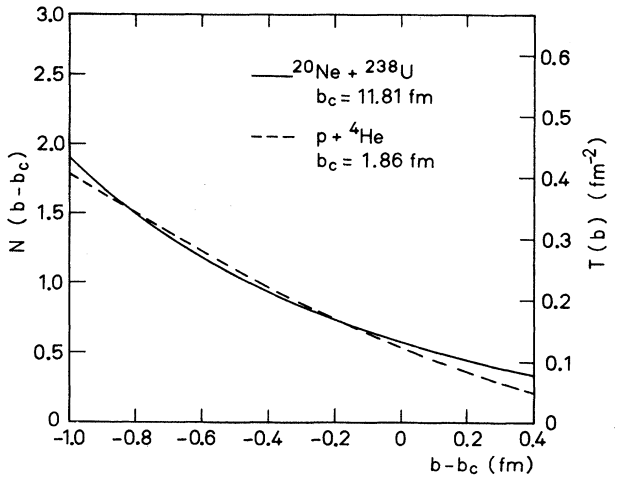

FIG. 3. The same two functions of Fig. 2, but plotted as a function of a shifted impact parameter $b-b_c$. Here, b_c is taken as $(\sigma^R/\pi)^{1/2}$, where σ^R is calculated as from Eq. (1) of the text.

B. Single nucleon removal in the Glauber picture

We now focus on the case of single nucleon removal, which begins to occur when $b\leq b_c$. For such a simple partial reaction cross section σ_G, we use the parametrization[2,18]

$$\sigma_G=2\pi\left[b_c-\frac{\Delta b}{2}\right]\Delta b \tag{11}$$

with the classical argument that impact parameters centered on $b_c-\Delta b/2$ with a width Δb contribute strongly to this channel, and other impact parameters contribute primarily to other channels. From Fig. 3, we crudely estimate $\Delta b\approx 0.4$–0.5 fm, since $N(b)>1$ implies increasing probability for two nucleon-nucleon collisions. To see this, we write the two collision probability P_2 as[18,19]

$$P_2\approx e^{-N(b)}(1-e^{-N(b)})^2\ . \tag{12}$$

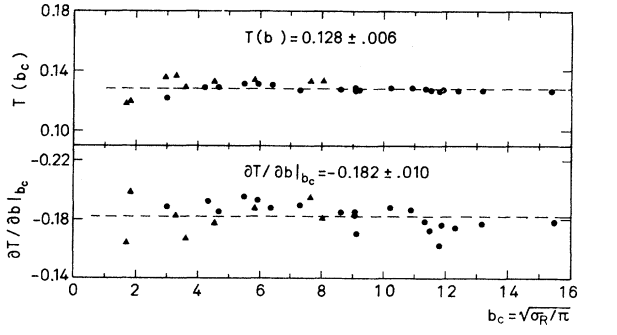

FIG. 4. Thickness function and its first derivative at b_c for the cases shown in Fig. 1. The average values are indicated by the dashed lines and the variances are given.

We find it peaks at $b-b_c \approx -0.6$ fm. The analogous peak for the single nucleon-nucleon collision probability function occurs at $b-b_c \approx -0.2$ fm. So, for the purpose of our simple geometrical model, it seems quite reasonable to take $\Delta b \approx 0.5$ fm. One could criticize the purely geometrical picture since the probability functions such as (10) are overlapping so that a single impact parameter has a distribution of channels to which it contributes. While this is true, the near constancy of $T(b_c)$ and $T'(b_c)$ suggests that *the relative contributions to all channels are the same in peripheral collisions.* Thus, (9) should be a valid first approximation to σ_G, where the method of picking the constant Δb is, perhaps, subject to debate. We feel that the model is incomplete at this stage, as no attempt has been made to correct for final state interactions (FSI). The FSI for single nucleon removal cross sections are a large correction to the Glauber model, and are therefore more significant than minor adjustments to the value Δb. In Sec. III, we develop a simple parametrization for this correction.

III. FINAL STATE INTERACTIONS

An important feature of nuclear reactions which is absent from the Glauber model is the role for final state interactions. To be specific, we address here the question of whether a nucleon struck on the surface of the nucleus escapes, and leaves the residual nucleus in a bound state. The incident nucleon is, therefore, believed to possess a reasonably straight trajectory and its FSI, if any, are neglected. We will make a rough estimate of the FSI of the struck nucleon based on geometrical considerations since we feel that a realistic calculation would require a Monte Carlo effort and would be well beyond the spirit of the present efforts.

Consider the possible recoil paths of a nucleon struck at radius b and the point P indicated in Fig. 5. We take P at the most probable collision point $z=0$, and let it define the vertex of a cone with its symmetry axis going through the center of the nucleus and its perpendicular intercept from the center of the nucleus equal to $b-\Delta b$. The line PR shows the edge of the cone with peak angle viewed in the y-z plane. When the nucleon recoils into the cone we say it will have the possibility of undergoing FSI. For a rough estimate, let us assume that a struck target nucleon can recoil isotropically in the z part of three-dimensional space. First, we need to know what fraction of this space is occupied by residual target matter. Let f represent this fraction of space. We then have

$$f=\frac{1}{4\pi}\int_0^{2\pi} d\phi \int_0^{\theta_{\max}} \sin\theta \, d\theta$$
$$=\tfrac{1}{2}(1-\cos\theta_{\max}) \, . \tag{13}$$

For our estimates we will consider typical values and for single nucleon knockout we will take

$$\sin\theta_{\max}=\frac{b_c-\Delta b}{b_c} \, . \tag{14}$$

Conversely, $(1-f)$ is the fraction of space free of FSI corrections.

Next, we consider the fact that the recoiling may not knock additional nucleons out of the target. This factor is dependent on the "thickness" of the target along the path taken by the recoiling nucleon. We approximate it by using the value of the average number of nucleons encountered in an inelastic nucleon-nucleus collision, which is defined by

$$\nu=\frac{B\sigma}{\sigma_{1B}^R} \, . \tag{15}$$

The average probability for a struck nucleon to escape the target without knocking out additional target nucleons is given by

$$P_{\rm esc}=[(1-f)+fe^{-\nu}] \, . \tag{16}$$

For very light targets, this tends towards unity, while for heavy targets it approaches 0.5. Thus our simple model cross section, including FSI, is given by

$$\sigma_G^F=\sigma_G P_{\rm esc} \, . \tag{17}$$

We now apply this simple version to the experimental data for (p,pn) at 400 MeV (Ref. 20) and at 2.1 GeV.[17] In these cases, we find the Coulomb dissociation contribution to be less than 3% of the Glauber result and therefore negligible. Figures 6 and 7 display calculated results from Eqs. (11) and (17) using $\Delta b=0.4$ fm and experimental (p,pn) data from Ref. 16. In order to apply the model to this channel we have multiplied σ_G and σ_G^F by the neutron to baryon ratio N/B of the target nucleus.

The basic parametrization $N\sigma/B$ is approximately correct only for the lightest nuclei. For the heaviest targets it exceeds the data by roughly a factor of 2. The inclusion of FSI through $P_{\rm esc}$ provides a dramatic improvement so that the general trend of the results is now reasonably reproduced. We still overpredict the cross section for heavier targets, but due to the limited data

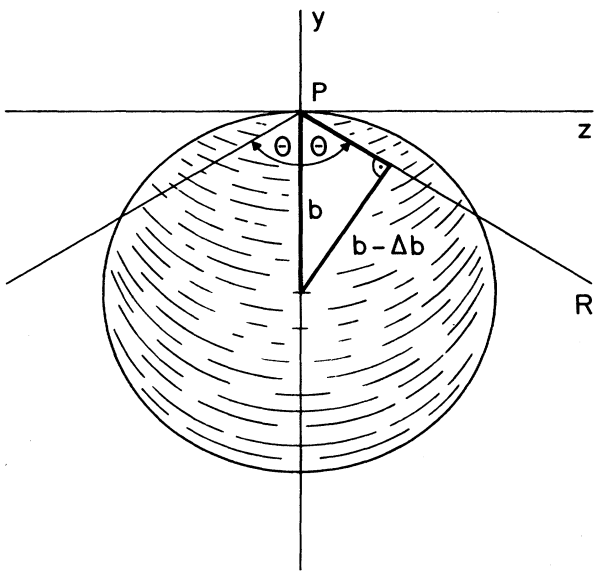

FIG. 5. Representation of the target nucleus with a nucleon struck at point P. The recoil paths included by the cone with angle θ between the surface and central axis are subject to corrections for FSI as discussed in the text.

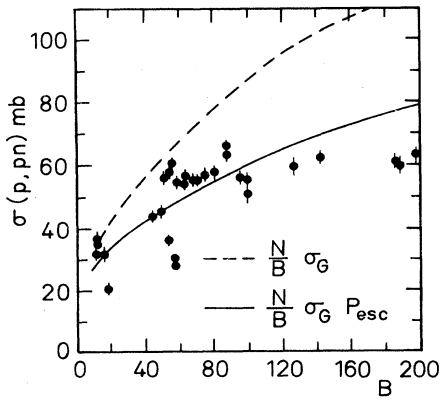

FIG. 6. Cross section for (p,pn) at 400 MeV as a function of target atomic number B. The data are taken from Ref. 21. The dashed curve represents the results of Eq. (11) scaled to the neutron removal channel as discussed in the text. The solid curve is the result when FSI are included.

and the simplicity of the model, we will now draw any strong conclusions from this discrepancy. It is interesting to note that the factor $NP_{\rm esc}/B$ used to modify σ_G is approximately constant (0.4 ± 0.04) for all the targets we have studied.

Note that the curves drawn in Figs. 6 and 7 are the same since there is no energy dependence in our simple model for the strong interaction processes except for variations in the nucleon-nucleon cross section which are weak. Furthermore, the changes in the nucleon-nucleon cross section enter only logarithmically and therefore we have felt free to neglect them here. In this regard it is encouraging that the data are also approximately energy independent.

The experiments at 400 MeV display sizable fluctuations in the vicinity of the magic and semimagic targets. Definite shell closure effects would be obtained within the Glauber model if more realistic neutron densities were employed. Such effects in the Ni isotopes were discussed extensively in Ref. 20. It remains to be shown that a more elaborate Glauber calculation with a Monte Carlo calculation of FSI will reproduce these fluctuations in detail.

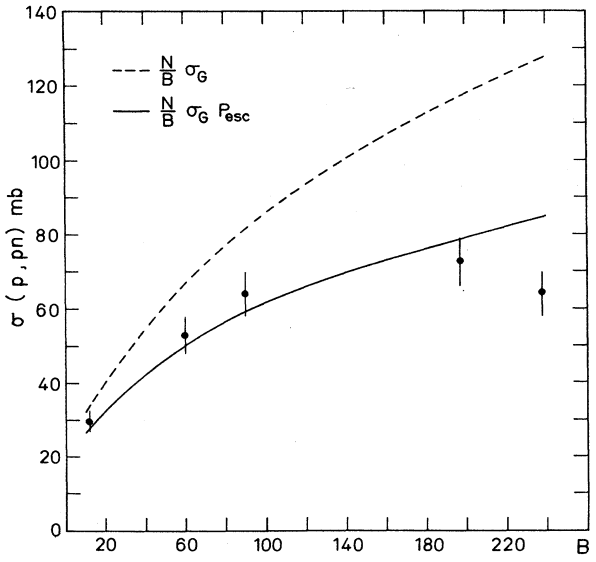

FIG. 7. Cross section for (p,pn) at 2.1 GeV as a function of target atomic number B. The data are from Ref. 17, and the dashed curves are the same as shown in Fig. 6, since negligible energy dependence is predicted by the model.

A more detailed study should also address the FSI due to pion production. Since the data show little energy dependence, one might deduce that pionic effects are small. On the other hand, the mean number of pions produced in nucleon-nucleon collisions at 2.1 GeV is of order 1. Thus, there is a nonnegligible probability that a produced pion will pass through the residual target matter. The interesting kinematical effect to note here is that the struck target nucleon will recoil with substantial longitudinal momentum when a pion is produced and this will greatly reduce its chance of undergoing FSI. Nevertheless, additional reductions in σ_G^F of order 20% may occur at high energies.

IV. COHERENT COULOMB/NUCLEAR DISSOCIATION

In this section, we review the Weizsacker-Williams (WW) approximation for the coherent dissociation of the target nucleus in the Coulomb and nuclear fields of a relativistic projectile. We shall present the derivation for the Coulomb piece in some detail, as we shall need some of the intermediate results in order to calculate interference effects later.

A. Review of the Weizsacker-Williams approximation for Coulomb fields

For our purposes, we assume that the projectile follows a straight line trajectory with impact parameter $b > b_c$. Under these conditions, the field of one nucleus at the center of another is primarily that of a photon, namely a transverse electromagnetic wave. We approximate the induced photoneutron cross section by

$$\sigma_{\rm WW} = \int_0^\infty N(E)\sigma_{\gamma n}(E)dE \ . \tag{18}$$

Here, $N(E)dE$ is the effective number of photons with energy between E and $E+dE$ taken in the WW approximation, and $\sigma_{\gamma n}$ is the cross section for photodisintegration resulting in the removal of one neutron from the target. The properties of these cross sections have been extensively studied. They are dominated by the giant dipole resonance (GDR) centered at 12 MeV in the heaviest nuclei, and increasing to 28 MeV in ^{4}He. Typically, the width of the resonance is 4–6 MeV. For light nuclei, the GDR deexcites by emission of a single neutron or proton, while for heavy nuclei, single and double neutron emission predominate. In the following, we shall exploit the fact that the GDR dominates the cross section in order to make a model for calculating nuclear-Coulomb interference effects. First, following Jackson and others,[21] we write the electric field seen at a point (r,θ,ϕ) in the target when a projectile of charge Z is incident with impact parameter b in the x direction and velocity v in the z direction

$$E_x(\mathbf{r},t)=\frac{\gamma Z(r\sin\theta\cos\phi-b)}{d^3}\ , \tag{19}$$

$$E_y(\mathbf{r},t)=\frac{\gamma Z r\sin\theta\cos\phi}{d^3}\ , \tag{20}$$

$$E_z(\mathbf{r},t)=\frac{\gamma Z(r\cos\theta+vt)}{d^3}\ , \tag{21}$$

where

$$d^2=(r\sin\theta\cos\phi-b)^2+r^2\sin^2\theta\sin^2\phi+\gamma^2(r\cos\theta+vt)^2\ . \tag{22}$$

Performing a Fourier transform in time, we get

$$E_x(\mathbf{r},\omega)=\left[\frac{2}{\pi}\right]^{1/2}\frac{Z\omega}{\gamma v^2 B(\theta,\phi)}(r\sin\theta\cos\phi)\times e^{-i\omega r\cos\theta/v}K_1\left[\frac{\omega B(\theta,\phi)}{\gamma v}\right], \tag{23}$$

$$E_y(\mathbf{r},\omega)=\left[\frac{2}{\pi}\right]^{1/2}\frac{Z\omega}{\gamma v^2 B(\theta,\phi)}r\sin\theta\sin\phi\times e^{-i\omega r\cos\theta/v}K_1\left[\frac{\omega B(\theta,\phi)}{\gamma v}\right], \tag{24}$$

$$E_z(\mathbf{r},\omega)=\left[\frac{2}{\pi}\right]^{1/2}\frac{iZ\omega}{\gamma^2 v^2}K_0\left[\frac{\omega B(\theta,\phi)}{\gamma v}\right], \tag{25}$$

where $B^2(\theta,\phi)=(r\sin\theta\cos\phi-b)^2+r^2\sin^2\theta\sin^2\phi$, and K_0,K_1 are modified Bessel functions.

Finally, we may break the field into its multipole components using the expansion

$$\mathbf{E}(\mathbf{r},\omega)=\sum_{lm}\left[\frac{i}{\omega}\nabla\times[a^E_{lm}(r,\omega)\mathbf{X}_{lm}]+a^M_{lm}(r,\omega)\mathbf{X}_{lm}\right], \tag{26}$$

where $\mathbf{X}_{lm}$ is a vector spherical harmonic. The coefficients we are interested in are the a^E_{lm}'s, which may be calculated using the formula

$$a^E_{lm}(r,\omega)=\frac{-\omega}{\sqrt{l(l+1)}}\int d\Omega\, Y^*_{lm}\,\mathbf{r}\cdot\mathbf{E}(\mathbf{r},\omega)\ . \tag{27}$$

For the problem at hand, $\omega r\ll 1$, so we may expand around $r=0$ to obtain

$$a^E_{10}=\frac{2iZ\omega^2 r}{\sqrt{3}\gamma^2 v^2}K_0\left[\frac{\omega b}{\gamma v}\right], \tag{28}$$

$$a^E_{11}=-a^E_{1-1}=\sqrt{\tfrac{2}{3}}\frac{Z\omega^2 r}{\gamma v^2}K_1\left[\frac{\omega b}{\gamma v}\right]. \tag{29}$$

The effective intensity, as a function of frequency, is given by

$$\frac{dI_{lm}}{d\omega\,2\pi b\,db}=\frac{1}{2\pi}\left|\frac{a^E_{lm}(r,\omega)}{a^E_{lm;\mathrm{PW}}(r,\omega)}\right|^2, \tag{30}$$

where

$$a^E_{lm;\mathrm{PW}}=i^{l-1}\frac{\sqrt{2\pi(2l+1)}}{(2l+1)!!}(\omega r)^l$$

is the appropriate expansion coefficient for a plane wave (PW) of unit intensity. Thus, we obtain

$$\frac{dI_{1,\pm1}}{d\omega\,2\pi b\,db}=\frac{1}{\pi^2}\frac{Z^2\omega^2}{\gamma^2 v^4}K_1^2\left[\frac{\omega b}{\gamma v}\right], \tag{31}$$

$$\frac{dI_{1,0}}{d\omega\,2\pi b\,db}=\frac{1}{\pi^2}\frac{Z^2\omega^2}{\gamma^4 v^4}K_0^2\left[\frac{\omega b}{\gamma v}\right], \tag{32}$$

in agreement with the usual result.[21] The function $N(E)$ appearing in Eq. (18) is then given by

$$N(\omega)=\frac{1}{\omega}I(\omega)=\frac{2Z^2}{\pi\omega v^2}\{xK_0(x)K_1(x)-v^2x^2[K_0^2(x)-K_1^2(x)]\} \tag{33}$$

with $x=\omega b/\gamma v$.

We shall evaluate the cross section two ways. First, we will use the experimentally measured γn cross section[22,23] to evaluate the integral (4.1) numerically. Alternately, we will evaluate the cross section using matrix elements of the Hamiltonian

$$H_1=-\frac{e}{2}\int d^3x\rho_1(\mathbf{x})\mathbf{x}\cdot\mathbf{E}(\mathbf{r},\omega)\ , \tag{34}$$

where $\rho_1=\rho_n-\rho_p$ for the target nucleus. To simplify matters, the matrix elements will be evaluated using the hydrodynamic model,[24] and assuming that the GDR dominates the cross section. The single neutron cross section is then given by the cross section for creating the GDR state multiplied by the branching ratio for the single neutron decay of the GDR, which we obtain phenomenologically from Ref. 22 as the ratio

$$\xi_{Br}=\frac{\sigma_{\gamma n}}{\sigma_\gamma}\ . \tag{35}$$

This procedure enables us to gauge the reliability of the matrix elements we shall use in Sec. IV B to calculate Coulomb-nuclear interference effects.

B. Coulomb-nuclear interference

While the Glauber model described in Sec. II is useful as a guide for estimating the incoherent contribution to the single nucleon removal cross section, it is unable to yield any information on the size of the interference between the Coulomb and strong amplitudes. In this section, we shall argue that such interference must occur, and that the size of the interference terms are not necessarily small for heavy projectiles. We shall then present a simple WW-based model for calculating the interference terms in heavy nuclei.

To begin, we simply note that the nucleon-nucleon interaction has an isovector component with range ≈ 0.6 fm. Calculations of the N-N potential[25] yield coupling constants of order unity. In optical models, an isovector interaction is responsible for part of the symmetry energy

in nuclei. If one assumes that the fields responsible for these forces are coupled to the isovector density ρ_1 via a Klein-Gordon equation, one finds that the coupling parameter is again of order unity, and that the field itself is proportional to $(N-Z)$. The existence of this field, whose $l=1$ component has the same quantum numbers as the photon, opens up the possibility that the nuclear and Coulomb amplitudes will interfere with one another. Physically, we expect to find interference even in the inclusive process we are studying here, as the electromagnetic contribution proceeds primarily through the decay of the intermediate GDR state, which may be excited by either the strong or Coulomb field of the projectile. Furthermore, it is not immediately obvious that the interference terms will be small, as they involve the product of a small strong interaction amplitude with a potentially large WW amplitude.

To model this, we assume that there is an interaction Hamiltonian of the form

$$H_S=\int d^3x\,\Phi_S(\mathbf{x},\omega)\rho_1(\mathbf{x},t)\ , \tag{36}$$

where the field Φ_S is the isovector field, which we assume transforms as a Lorentz scalar. We shall proceed to calculate the field seen by the target by a procedure formally identical to the WW method outlined previously. In the projectile rest frame, we assume that the field outside the projectile is given by a Yukawa form

$$\Phi_S(\mathbf{r})=\frac{g_P e^{-\mu(r-R_P)}}{r}\ , \tag{37}$$

where g_P is a strength parameter, $\mathbf{r}=0$ at the projectile's center, R_P is the projectile radius, and the prime indicates that we are in the projectile rest frame. Boosting to the laboratory frame, the target sees a field given by

$$\Phi_S(\mathbf{r},t)=\frac{g_P e^{-\mu(d-R_p)}}{d}\ , \tag{38}$$

where d is defined in Sec. V. Fourier transforming in time, we get

$$\Phi_S(\mathbf{r},\omega)=\frac{g_P e^{\mu R_p}}{\sqrt{2\pi}\gamma v}e^{-i\omega r\cos\theta/\gamma v}K_0[mB(\theta,\phi)]\ , \tag{39}$$

where $m^2=\mu^2+\omega^2/\gamma^2v^2$.

As we discussed previously, we expect $\mu\approx 300$ MeV, and

TABLE I. Weizsacker-Williams and hydrodynamic model cross sections for single neutron removal from ^{197}Au. Also shown is the Coulomb-nuclear interference term for $\lambda=1-2$.

Projectile	Energy/nucleon (GeV)	σ_{WW} (mb)	σ_{hyd} (mb)	σ_{int} (mb)
^{12}C	2.1	40	25	0
^{20}Ne	2.1	104	90	0
^{40}Ar	1.8	295	316	0.3–0.6
^{56}Fe	1.7	569	650	0.5–1
^{139}La	1.26	2058	2188	5–10
^{238}U	0.96	4148	3779	13–25

TABLE II. Single neutron removal cross sections for ^{12}C projectiles at 2.1 GeV/nucleon.

Target	σ_G^F (mb)	σ_{WW} (mb)	σ_{Tot} (mb)	σ_{exp}
^{12}C	64±3	0.51	65±3	60.9±0.6
^{59}Co	91±5	8	99±5	89±5
^{89}Y	102±5	17	119±5	115±6
^{197}Au	128±6	40	168±6	178±7
^{238}U	136±7	24	160±7	173±22

TABLE III. Single neutron removal cross sections for ^{20}Ne projectiles at 2.1 GeV/nucleon.

Target	σ_G^F (mb)	σ_{WW} (mb)	σ_{Tot} (mb)	σ_{exp}
^{12}C	71±4	1.3	72±4	78±2
^{59}Co	98±5	21	109±5	132±7
^{89}Y	109±5	42	151±5	160±7
^{197}Au	134±7	104	238±7	268±11
^{235}U	142±7	63	205±7	192±16

TABLE IV. Single neutron removal cross sections for ^{40}Ar projectiles at 1.8 GeV/nucleon.

Target	σ_G^F (mb)	σ_{WW} (mb)	σ_{Tot} (mb)	σ_{exp}
^{89}Y	121±6	115	236±6	283±11
^{197}Au	146±7	295	441±7	463±30

TABLE V. Single neutron removal cross sections for ^{56}Fe projectiles at 1.7 GeV/nucleon.

Target	σ_G^F (mb)	σ_{WW} (mb)	σ_{Tot} (mb)	σ_{exp}
^{12}C	91±5	7	98±5	94±2
^{59}Co	117±6	113	230±6	194±9
^{89}Y	127±6	222	349±6	353±14
^{197}Au	153±7	569	722±7	707±52

TABLE VI. Single neutron removal cross sections for ^{139}La projectiles at 1.26 GeV/nucleon.

Target	σ_G^F (mb)	σ_{WW} (mb)	σ_{Tot} (mb)	σ_{exp}
^{12}C	119±6	24	143±6	148±2
^{59}Co	148±7	376	524±7	450±30
^{197}Au	183±9	2058	2241±9	2130±120

TABLE VII. Single neutron removal cross section for ^{238}U projectiles at 0.96 GeV/nucleon.

Target	σ_G^F (mb)	σ_{WW} (mb)	σ_{Tot} (mb)	σ_{exp}
^{197}Au	198±10	4148	4346	NA

$$g_P \approx \frac{\lambda(N_P - Z_P)}{A_p^{\alpha}} , \tag{40}$$

with $\lambda \approx 1-2$. The exponent of A_P in this equation is determined by the precise form of the source term in the equations that determine Φ_S. For a Klein-Gordon equation coupled to a uniformly distributed, spherical density $\rho_1 = [(N_p - Z_p)/A_p]\rho_0 \Theta(R_p - r)$, we obtain $\alpha = \frac{2}{3}$. For the more realistic case with the neutron excess concentrated near the surface of the nucleus, we obtain $\alpha = \frac{1}{3}$. We shall use this value in the calculations that follow.

Using the hydrodynamic model, we calculate the WW cross section and the interference term. The results are shown in Table I for a variety of projectiles on a Au target. Also shown is the standard WW cross section. We see that the simple model described here reproduces the WW results to within 5–10%, and that the interference terms are less than 25 mb even for the heaviest projectiles. The uncertainties in the measured cross sections for heavy projectiles are roughly 100 mb, and we therefore conclude that the interference terms cannot be seen in the current experiments. In Sec. V, we shall neglect the interference terms.

V. RESULTS AND CONCLUSIONS

In this section, we compare the results of our calculations with experimental data taken from Ref. 3. The data are compared to the sum of the WW cross section obtained by evaluating Eq. (18) numerically with the tabulated values of $\sigma_{\gamma n}$ from Ref. 22 and the Glauber cross section taken from Sec. II with $\Delta b = 0.5$ fm $\pm 5\%$. The results are shown in Tables II-VII for a variety of projectiles and targets. We find good agreement between theory and experiment for nearly all cases considered, with the notable exception of cases involving ^{59}Co targets. It is encouraging that we are able to obtain this level of agreement with the very simple models we have used.

The fact that the deviations occur almost exclusively in the ^{59}Co targets suggests that the problem does not lie in the WW approximation, but rather in a source specific to Co. One possibility is that there is a normalization error in the tabulated γn data, similar to the 7% error in the normalization of the ^{197}Au cross section.[26] This notion receives some support from the fact that the ratios of the observed Coulomb dissociation cross sections roughly agree with the ratios predicted by the WW approximation. We therefore conclude that the WW approximation provides a reasonable description of the data, and that the apparent deviations measured in Ref. 3 are not a signal of new physics, but rather reflect the uncertainties inherent in the separation of the nuclear contribution to single nucleon removal cross section, and possible systematic errors in the γn cross sections used to calculate the WW cross section.

Finally, we would like to emphasize the possibility that the interference effects calculated in Sec. II of this paper are comparable to the uncertainties in the current round of experiments. This raises the possibility that improved experiments may be able to measure these terms, providing useful information on the isovector components of the nuclear field.

This work was supported by the U.S. Department of Energy under Contract No. DE-FG02-87ER40371, Division of High Energy and Nuclear Physics.

[1]H. H. Heckman and P. J. Lindstrom, Phys. Rev. Lett. **37**, 56 (1976); D. L. Olson *et al.*, Phys. Rev. C **24**, 1529 (1981).

[2]T. K. Gaisser, T. Stanev, P. Freier, and C. J. Waddington, Phys. Rev. D **25**, 2341 (1982); D. L. Olson *et al.*, Phys. Rev. C **28**, 1602 (1983).

[3]M. T. Mercier *et al.*, Phys. Rev. C **33**, 1655 (1986); J. C. Hill, F. K. Wohn, J. A. Winger, and A. R. Smith, Phys. Rev. Lett. **60**, 999 (1988); Phys. Rev. C **38**, 1722 (1988).

[4]R. J. Glauber, in *High Energy Physics and Nuclear Structure*, edited by G. Alexander (North-Holland, Amsterdam, 1967), p. 311.

[5]W. Czyz and L. C. Maximon, Ann. Phys. (N.Y.) **52**, 59 (1969).

[6]G. Faldt, H. Pilkhun, and H. G. Schaile, Ann. Phys. (N.Y.) **82**, 326 (1974). For more recent reviews see G. F. Bertsch and S. D. Gupta, Phys. Rep. **160**, 189 (1988) and B. Schurmann, W. Zwermann, and R. Malfeit, *ibid.* **147**, 1 (1987).

[7]T. W. Donnely, J. Dubach, and J. D. Walecka, Nucl. Phys. **A232**, 355 (1974).

[8]P. M. Fishbane and J. S. Trefil, Phys. Rev. Lett. **32**, 396 (1974).

[9]V. Franco, Phys. Rev. Lett. **32**, 911 (1974).

[10]W. L. Wang and R. G. Lipes, Phys. Rev. C **9**, 814 (1974).

[11]S. Barshay, C. B. Dover, and J. P. Vary, Phys. Rev. C **11**, 360 (1975).

[12]P. J. Karol, Phys. Rev. C **11**, 1203 (1975).

[13]H. L. Bradt and B. Peters, Phys. Rev. **77**, 54 (1950).

[14]J. Blocki, J. Randrup, W. J. Swiatecki, and C. F. Tsang, Ann. Phys. (N.Y.) **105**, 427 (1977).

[15]H. R. Collard, L. R. B. Elton, and R. Hofstadter, in *Landolt-Bornstein: Numerical Data and Functional Relationships in Science and Technology*, edited by K. H. Hellwege and H. Schopper (Springer, Berlin, 1967), Group I, Vol. 2, p. 21, and references therein.

[16]J. A. Jaros, Lawrence Berkeley Laboratory Report No. LBL-3849 (unpublished).

[17]P. J. Karol and J. M. Miller, Phys. Rev. **166**, 1089 (1968).

[18]J. Hufner, K. Schafer, and B. Schurmann, Phys. Rev. C **12**, 1888 (1975).

[19]J. Vary, Phys. Rev. Lett. **40**, 295 (1978).

[20]M. T. Mercier, J. C. Hill, F. K. Wohn, and A. R. Smith, Bull. Am. Phys. Soc. **27**, 540 (1982); M. T. Mercier, Ph.D. thesis, Iowa State University, 1982.

[21]J. D. Jackson, *Classical Electrodynamics* (Wiley, New York, 1975); A. Goldberg, Nucl. Phys. **A240**, 636 (1984); A. Winther and K. Adler, *ibid.* **A319**, 518 (1979); C. A. Bertulani and G. Baur, *ibid.* **A442**, 739 (1985).

[22]B. L. Berman, Atlas of Photoneutron Cross Sections, University of California Report No. UCRL-78482, and references therein.

[23]Digital Data Library, Photonuclear Data Center, Office of Standard Reference Data, National Bureau of Standards,

Washington, D. C. 20234.
[24]A. Bohr and B. Mottelson, *Nuclear Structure* (Benjamin, Reading, Mass., 1975), Vol. 2.
[25]R. Machleidt, K. Holinde, and Ch. Elster, Phys. Rep. **149**, 1 (1987); M. Lacomb, B. Loiseau, J.-M. Richard, R. Vinh Mau, J. Cote, P. Pires, and R. deTourreil, Phys. Rev. C **21**, 861 (1980).
[26]B. L. Berman, R. E. Pywell, S. S. Dietrich, M. N. Thompson, K. G. Mcneill, and J. W. Jury, Phys. Rev. C **36**, 1286 (1987).